Proceedings of the 7th World Congress on Momentum, Heat and Mass Transfer (MHMT'22)
~~Lisbon, Portugal~~ Virtual Conference– April 07 – 09, 2022
Paper No. ENFHT 199
DOI: 10.11159/enfht22.199

Spreading Dynamics of Al_2O_3-Water Nanofluid Droplets Impacting On a Smooth Flat Surface

Yunus T. Aksoy[1], Pinar Eneren[1], Erin Koos[2], Maria Rosaria Vetrano[1]
[1]KU Leuven, Department of Mechanical Engineering, Division of Applied Mechanics and Energy Conversion (TME)
B-3001 Leuven, Belgium
yunus.aksoy@kuleuven.be; pinar.eneren@kuleuven.be; rosaria.vetrano@kuleuven.be
[2]KU Leuven, Department of Chemical Engineering, Soft Matter, Rheology and Technology (SMaRT)
B-3001 Leuven, Belgium
erin.koos@kuleuven.be

Abstract This research focuses on the maximum spreading diameters of Al_2O_3-water nanofluid droplets and their comparison with available literature models for pure liquids based on the energy conservation principle. In total, 978 data points are acquired for three different nanoparticle concentrations in various aqueous glycerol solutions. To ensure accuracy, each sample is experimentally characterized before the droplet impact measurements in terms of stability, density, viscosity, and surface tension. We demonstrate that nanofluid droplets exhibit different spreading dynamics with respect to pure liquids. That is, the models formulated for the pure liquids cannot directly predict the maximum spreading factor for the nanofluid droplets, and the underprediction can even reach up to 45%.

***Keywords*:** droplet impact, droplet spreading, nanofluid spreading, nanofluid droplet

1. Introduction

Nanofluids have drawn significant attention from researchers owing to their superior thermal properties and potential applications in various fields [1]. From extensive research, nanofluids possess significantly higher thermal features than base liquids despite the controversies and scattered experimental data [2]. Hence, it is undisputed that nanofluids can potentially be employed as advanced coolants in near future [3].

Similarly, droplet impact onto a solid surface still receives considerable interest from both academia and industry as it takes place in numerous technological applications, such as ink-jet printing, spin coating, spray painting, and even for bloodstain pattern analysis on crime scenes [4]–[7].

The dynamics of a spreading droplet is described with the non-dimensional numbers [8]: the Weber number $\mathrm{We} = \rho D_0 u_0^2/\sigma$ (inertia/surface tension forces), the Reynolds number $\mathrm{Re} = \rho u_0 D_0/\eta$ (inertia/viscous forces), and the Ohnesorge number $\mathrm{Oh} = \mathrm{We}^{0.5}/\mathrm{Re}$ (viscous forces/inertia and surface tension forces), where the fluid properties such as density, surface tension, and dynamic viscosity are represented by ρ, σ, and η, respectively, and impact properties such as droplet diameter upon impact and impact speed are denoted by D_0 and u_0.

2. Materials and experimental methodology

A systematic and repeatable experimental approach is followed, covering wide ranges of Weber and Reynolds numbers. In total, 978 data points are collected from 42 sets of experiments, each with a constant Ohnesorge number.

2.1. Preparation, stabilization, and characterization of nanofluids

Nanofluids with three mass concentrations ($\phi = 0.01$ wt.%, 0.1 wt.%, and 1 wt.%) are obtained by diluting an unstabilized commercial water-based dispersion from Sigma-Aldrich that contains 20 wt.% Al_2O_3 nanoparticles with an average diameter of 45 nm (TEM) in aqueous glycerol. The aqueous glycerol solutions are prepared by mixing 99.98% pure glycerol (Acros Organics) with milli-q water. The glycerol concentration ω_G is then calculated as the mass ratio of the glycerol to the total mass of the nanofluid. The final dilution is achieved by mixing via a speed-mixer (SpeedMixer, DAC 150.1 FVZ) and a shaker platform (Heidolph, PROMAX 2020) until well dispersed. The base suspension contains no

dispersant, and no surfactant is added during the dilution process. Using this protocol, 23 samples of nanofluids are prepared with glycerol concentrations ranging from 0% to 80%. These samples are labelled with the following X-ω_G-nf-ϕ where X represents the nature of the base liquid, i.e., water (W) or aqueous glycerol (AG).

To accurately calculate the Weber and Reynolds numbers, the nanofluid properties, i.e., the density, viscosity, and surface tension, are all measured and given in Table 1. The dynamic viscosity measurements are conducted on the ARES-G2 rheometer using a double-walled Couette cell at shear rates between 1 to 100 s^{-1}, within 3% uncertainty, and the nanofluids display Newtonian behavior. The pendant drop method is employed on a KSV CAM200 goniometer for the surface tension measurements. The Young-Laplace fit is applied to 150 images for each sample: 30 consecutive images out of 5 droplets are averaged to confirm that the surface tension is invariant from droplet to droplet and independent of the pending time. For the density measurements, a pycnometer (BlauBrand, Gay-Lussac pattern, 10.109 ml) is used.

Table 1: Material properties: glycerol mass fraction in water (ω_G), mass fraction of nanoparticles (ϕ), surface tension (σ), density (ρ), and dynamic viscosity (η).

Sample	ω_G $[wt\%]$	ϕ $[wt\%]$	σ $\left[\frac{mN}{m}\right]$	ρ $\left[\frac{kg}{m^3}\right]$	η $[mPa \cdot s]$
W-nf-0.01	0	0.01	70.2	996.7	1.0
AG-30-nf-0.01	30	0.01	69.9	1070.6	2.5
AG-37-nf-0.01	37	0.01	68.5	1087.9	3.4
AG-43-nf-0.01	43	0.01	67.6	1103.1	4.2
AG-58-nf-0.01	58	0.01	67.3	1145.5	9.9
AG-70-nf-0.01	70	0.01	66.1	1178.0	23.4
AG-75-nf-0.01	75	0.01	65.5	1190.2	36.3
AG-80-nf-0.01	80	0.01	64.7	1204.5	60.6
W-nf-0.1	0	0.1	71.4	995.9	1.0
AG-30-nf-0.1	30	0.1	70.0	1071.1	2.6
AG-37-nf-0.1	37	0.1	69.1	1086.8	3.5
AG-43-nf-0.1	43	0.1	68.3	1101.4	4.2
AG-58-nf-0.1	58	0.1	67.2	1144.1	9.2
AG-70-nf-0.1	70	0.1	65.9	1178.2	23.3
AG-75-nf-0.1	75	0.1	65.0	1190.6	35.6
AG-80-nf-0.1	80	0.1	64.8	1204.3	62.0
AG-30-nf-1	30	1	69.2	1080.0	2.6
AG-37-nf-1	37	1	69.3	1097.6	3.5
AG-43-nf-1	43	1	67.9	1115.3	4.6
AG-58-nf-1	58	1	66.7	1154.1	10.8
AG-70-nf-1	70	1	65.4	1184.3	24.6
AG-75-nf-1	75	1	65.1	1200.1	40.9
AG-80-nf-1	80	1	64.8	1214.8	69.6

The stability of nanofluids is crucial for both the repeatability and reliability of the experiments. Therefore, we confirm the temporal stability of our samples using TurbiScan MA2000. We analyze the light transmittance for low mass fraction nanofluids ($\phi = 0.01$ wt.% and 0.1 wt.%). For the higher mass fraction of $\phi = 1$ wt.%, the light back-scattering is measured due to the strong light extinction. The turbidity scan index TSI [9] is calculated to evaluate the temporal stability quantitatively by examining the variation in the transmittance or back-scattering data. To be on the safe side for the stability, the duration of the experiments is constrained to 4 hours ($TSI \ll 0.015$), which corresponds to a change of less than 3% in the back-scattering along the tube length [10].

The main contributions to uncertainties in these numbers derive from the nanofluid viscosity and the image post-processing for the droplet diameters and their impact velocities. Consequently, the uncertainty values on the governing parameters and the non-dimensional groups (η, D_0, u_0, Re, and We) are estimated as 3%, 0.2%, 0.8%, 3.4%, and 2.1%, respectively.

2.2. Experimental setup and conditions

The schematic of the experimental setup is shown in Fig. 1. The working fluid is infused from a syringe pump (Harvard 4400 PHD) through a tube to a blunt-tip needle where a droplet is formed. Two needles (GA 30 and GA 22) are are used to alter the droplet size from 2.2 to 2.8 mm. The droplet falls onto a 3-cm diameter smooth sapphire substrate. A laser-photo-diode unit creates a light beam through which the droplet passes and triggers the image acquisition unit composed of a high-speed camera (Photron Fast-CAM) and a Light-emitting diode (LED) illumination. The images are acquired at 12,000 fps in 10-bit grey-scale and with 29 µs shutter time. The test section is enclosed with a transparent Plexiglas box to prevent splashing of droplets and reduce the influence of air currents. The roughness of the sapphire substrate is measured by Mitutoyo CS-3200 with an average roughness R_a of 0.00909 µm and roughness pitch of 0.001 µm.

Fig. 1: Schematic of the experimental setup characterizing the droplet dynamics.

3. Mathematical models based on energy-balance equation

To calculate the maximum spreading factor β_{max}, energy conservation should be satisfied upon droplet impact (kinetic energy K_1 and surface-free energy S_1) and at the maximum spreading (kinetic energy K_2, surface-free energy S_2, and viscous dissipation W), as given in Eqn. 1. Assuming that the droplet is cylindrical at its maximum diameter D_m with a rim thickness h_m, each energy term can be inserted into the energy balance as shown in Eqn. 2:

$$K_1 + S_1 = K_2 + S_2 + W, \tag{1}$$

$$\frac{\pi\rho u_0^2 D_0^3}{12} + \pi D_0^2\sigma = 0 + \pi\sigma D_m h_m + \frac{\pi}{4}\sigma D_m^2(1-\cos\theta) + \eta\left(\frac{u_c}{L_c}\right)^2 V_c t_m. \tag{2}$$

where θ is the contact angle, L_c and u_c are the characteristic length and velocity, respectively. V_c and t_m denote the volume and time in which the viscous dissipation occurs.

Pasandideh et al. [11] solve this energy equation neglecting the lateral surface energy at the maximum spreading. The characteristic length in this model is also assumed to be equal to the boundary layer thickness at the solid-liquid interface, i.e., $L_c = \frac{2D_0}{\sqrt{\mathrm{Re}}}$ in Eqn.3:

$$\beta_{max} = \sqrt{\frac{\mathrm{We}+12}{3(1-\cos\theta)+4\left(\frac{\mathrm{We}}{\sqrt{\mathrm{Re}}}\right)}}. \tag{3}$$

Ukiwe et al. [12] adapt this model by updating the surface energy term and come up with Eqn.4:

$$(\mathrm{We}+12)\beta_{max} = 8 + \beta_{max}^3\left(3(1-\cos\theta)+4\left(\frac{\mathrm{We}}{\sqrt{\mathrm{Re}}}\right)\right). \tag{4}$$

With the recent developments, the characteristic length and velocity models [13] are also improved as well as time scales [14]. Du et al. [15] incorporate new parameters to more accurately calculate β_{max} (Eqn.5), by improving the viscous dissipation term, which is often overpredicted:

$$(\mathrm{We}+12)\beta_{max} = 8 + 3(1-\cos\theta)\beta_{max}^{3} + 0.98\frac{\mathrm{We}^{1.06}}{\mathrm{Re}}\beta_{max}^{6.5}. \quad (5)$$

4. Results & discussion

Fig. 2 shows how the three aforementioned models fit our experimental data for the three tested nanofluid concentrations. It is clear from those graphs that the Al_2O_3 nanofluids show different characteristics than that of the liquids without nanoparticles, especially in the more viscous regime. Although all models fail to predict the nanofluid spreading factor accurately, the model of Du et al. [15] yields the best results owing to the improved viscous dissipation term. Therefore, a more extensive model is required to include the impact of the presence of the nanoparticles on the maximum spreading factor.

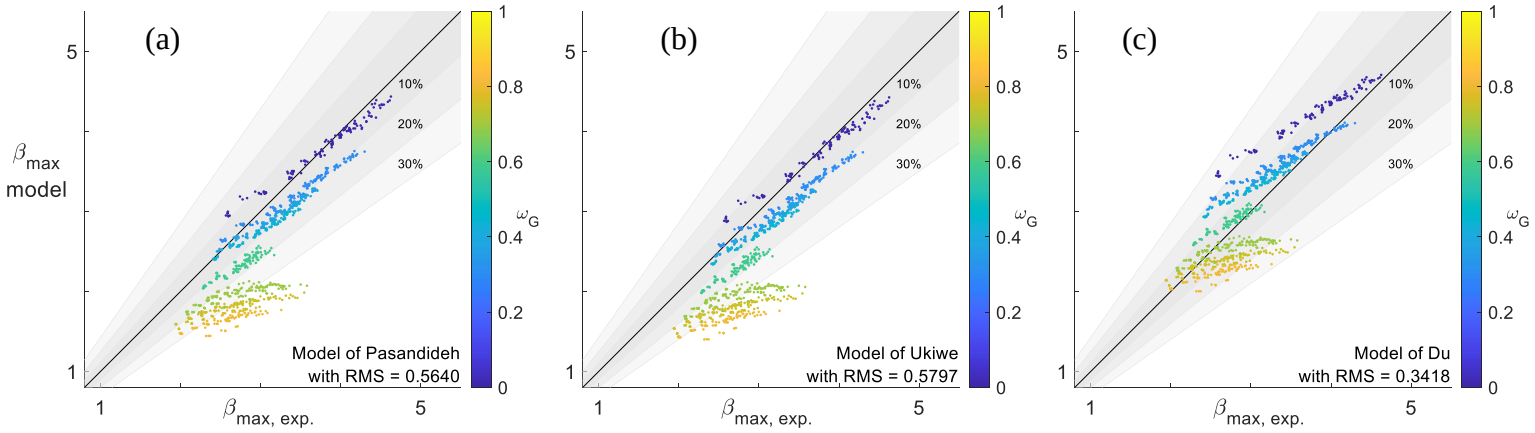

Fig. 2: The misestimation of some literature models formulated for pure liquids on the maximum spreading factor (β_{max}) of nanofluid droplets based on the current experimental work: Models of (a) Pasandideh et al. [11] with RMS = 0.564, (b) Ukiwe et al. [12] with RMS = 0.5797 (c) Du et al. [15] with RMS = 0.3418. The error-bands of 10%, 20%, and 30% are plotted in grey color.

5. Conclusion

In this experimental work, it is demonstrated that nanofluid droplets spread differently compared to pure liquid droplets. In other words, the models formulated for the pure liquids cannot correctly predict the maximum spreading factor for the nanofluid droplets. The difference between the model predicted values and experiment results can even reach up to 45%, and a new model should be implemented for these engineering fluids. It can be concluded that the presence of nanoparticles has an impact on the droplet's spreading dynamics, which requires a better understanding of the droplet spreading phenomenon.

Acknowledgements

The authors gratefully acknowledge the in-kind support of Department of Chemical Engineering, KU Leuven. This work was supported by Interne Fondsen KU Leuven / Internal Funds KU Leuven (C24/18/057).

References

[1] S. M. S. Murshed, C. A. Nieto De Castro, M. J. V. Loureno, M. L. M. Lopes, and F. J. V. Santos, "A review of boiling and convective heat transfer with nanofluids," *Renew. Sustain. Energy Rev.*, vol. 15, no. 5, pp. 2342–2354, 2011, doi: 10.1016/j.rser.2011.02.016.

[2] Y. T. Aksoy, Y. Zhu, P. Eneren, E. Koos, and M. R. Vetrano, "The impact of nanofluids on droplet/spray cooling of a heated surface: A critical review," *Energies*, vol. 14, no. 1, pp. 1–34, 2021, doi: 10.3390/en14010080.

[3] S. M. S. Murshed and C. A. N. de Castro, “Nanofluids as Advanced Coolants,” in *Green Solvents I: Properties and Applications in Chemistry*, A. Mohammad, Ed. Dordrecht: Springer Netherlands, 2012, pp. 397–415.
[4] A. L. Yarin, “Drop impact dynamics: Splashing, spreading, receding, bouncing..,” *Annu. Rev. Fluid Mech.*, vol. 38, pp. 159–192, 2006, doi: 10.1146/annurev.fluid.38.050304.092144.
[5] P. Galliker, J. Schneider, H. Eghlidi, S. Kress, V. Sandoghdar, and D. Poulikakos, “Direct printing of nanostructures by electrostatic autofocussing of ink nanodroplets,” *Nat. Commun.*, vol. 3, no. May, 2012, doi: 10.1038/ncomms1891.
[6] R. Rioboo, C. Tropea, and M. Marengo, “Outcomes from a drop impact on solid surfaces,” *At. Sprays*, vol. 11, no. 2, pp. 155–165, 2001, doi: 10.1615/AtomizSpr.v11.i2.40.
[7] N. Laan, K. G. De Bruin, D. Bartolo, C. Josserand, and D. Bonn, “Maximum diameter of impacting liquid droplets,” *Phys. Rev. Appl.*, vol. 2, no. 4, pp. 1–7, 2014, doi: 10.1103/PhysRevApplied.2.044018.
[8] C. Mundo, M. Sommerfeld, and C. Tropea, “Droplet-wall collisions: Experimental studies of the deformation and breakup process,” *Int. J. Multiph. Flow*, vol. 21, no. 2, pp. 151–173, 1995, doi: 10.1016/0301-9322(94)00069-V.
[9] B. Q. Li, C. Zou, H. Liang, W. Chen, S. Lin, and Y. Liao, “Mass transfer from nanofluid single drops in low interfacial tension liquid–liquid extraction process,” *Chem. Phys. Lett.*, vol. 771, no. March, p. 138530, 2021, doi: 10.1016/j.cplett.2021.138530.
[10] Y. T. Aksoy, P. Eneren, E. Koos, and M. R. Vetrano, “Spreading-splashing transition of nanofluid droplets on a smooth flat surface,” *J. Colloid Interface Sci.*, vol. 606, pp. 434–443, 2022, doi: 10.1016/j.jcis.2021.07.157.
[11] M. Pasandideh-Fard, Y. M. Qiao, S. Chandra, and J. Mostaghimi, “Capillary effects during droplet impact on a solid surface,” *Phys. Fluids*, vol. 8, no. 3, pp. 650–659, 1996, doi: 10.1063/1.868850.
[12] C. Ukiwe and D. Y. Kwok, “On the maximum spreading diameter of impacting droplets on well-prepared solid surfaces,” *Langmuir*, vol. 21, no. 2, pp. 666–673, 2005, doi: 10.1021/la0481288.
[13] Y. Yonemoto and T. Kunugi, “Analytical consideration of liquid droplet impingement on solid surfaces,” no. April, pp. 1–11, 2017, doi: 10.1038/s41598-017-02450-4.
[14] S. Lin, B. Zhao, S. Zou, J. Guo, Z. Wei, and L. Chen, “Journal of Colloid and Interface Science Impact of viscous droplets on different wettable surfaces : Impact phenomena , the maximum spreading factor , spreading time and post-impact oscillation,” *J. Colloid Interface Sci.*, vol. 516, pp. 86–97, 2018, doi: 10.1016/j.jcis.2017.12.086.
[15] J. Du, X. Wang, Y. Li, Q. Min, and X. Wu, “Analytical Consideration for the Maximum Spreading Factor of Liquid Droplet Impact on a Smooth Solid Surface,” *Langmuir*, vol. 37, no. 24, pp. 7582–7590, 2021, doi: 10.1021/acs.langmuir.1c01076.